Acta Oceanol. Sin., 2014, Vol. 33, No. 12, P. 24–31
DOI: 10.1007/s13131-014-0551-1
http://www.hyxb.org.cn
E-mail: hyxbe@263.net

An impact assessment of sea ice on ocean optics observations in the marginal ice zone of the Arctic

LI Tao[1], ZHAO Jinping[1,2]*

[1] Ocean University of China, Qingdao 266100, China
[2] Physical Oceanography Laboratory, Ocean University of China, Qingdao 266100, China

Received 18 June 2013; accepted 3 June 2014

Abstract

Diffuse attenuation coefficient (DAC) of sea water is an important parameter in ocean thermodynamics and biology, reflecting the absorption capability of sea water in different layers. In the Arctic Ocean, however, sea ice affects the radiance/irradiance measurements of upper ocean, which results in obvious errors in the DAC calculation. To better understand the impacts of sea ice on the ocean optics observations, a series of *in situ* experiments were carried out in the summer of 2009 in the southern Beaufort Sea. Observational results show that the profiles of spectral diffuse attenuation coefficients of seawater near ice cover within upper surface of 50 m were not contaminated by the sea ice with a solar zenith angle of 55°, relative azimuth angle of $110° \leqslant \varphi \leqslant 115°$ and horizontal distance between the sensors and ice edge of greater than 25 m. Based on geometric optics theory, the impact of ice cover could be avoided by adjusting the relative solar azimuth angle in a particular distance between the instrument and ice. Under an overcast sky, ice cover being 25 m away from sensors did not affect the profiles of spectral DACs within the upper 50 m either. Moreover, reliable spectral DACs of seawater could be obtained with sensors completely covered by sea ice.

Key words: impact assessment, optical observation, ice edge, Arctic Ocean

Citation: Li Tao, Zhao Jinping. 2014. An impact assessment of sea ice on ocean optics observations in the marginal ice zone of the Arctic. Acta Oceanologica Sinica, 33(12): 24–31, doi: 10.1007/s13131-014-0551-1

1 Introduction

The marginal ice zone (MIZ) in the Arctic is an important transitional region from open water to pack ice where strong interactive air-ice-sea radiative transfer processes occur, resulting in a complex radiation environment. Over the past 30 years, the properties of the radiative transfer in the MIZ have been changing because of the remarkable reduction in both the thickness and extent of sea ice, particularly the replacement of perennial sea ice with annual sea ice (Deser and Teng, 2008; Haas et al., 2008; Kwok et al., 2009; Kwok and Rothrock, 2009). The horizontal extent and concentration of sea ice affect both the surface reflectivity and absorption of a shortwave energy with depth in the ocean's upper mixed layer. Therefore, the ocean optics observations in the MIZ need us to improve our understanding of the surface radiation energy balance and upper-ocean thermodynamics. In addition, the light field structure in the MIZ is also a critical factor affecting ecosystem dynamics involving ice algae, which is a major component of primary production. Moreover, accurate calculations of the optical properties in the MIZ are a requirement for more effective uses of remote sensing observations of these surfaces.

However, the ocean optics observations near the ice edge in the MIZ are often affected by sea ice, leading to some degree of error in diffuse attenuation coefficient (DAC) calculations from the contaminated optics data. To avoid these impacts, optical sensors are typically deployed as far from the ice cover as possible. In some cases, it is impossible to make optical measurements without the impact of the ice cover (e.g., in the area with an ice concentration of more than 90%). To the best of our knowledge, there have been no studies or field efforts to assess the impacts of the ice cover on the ocean optics measurements in the MIZ.

At times, the platform on which the observations are based affects the ambient underwater light fields as well, depending on a solar zenith angle θ and relative azimuth angle φ, the single scatter albedo and the distance between the platform and the sensors (Gordon, 1985). An upwelling radiance can decrease by 10%–20% if doing the optic profile measurement with a distance of less than 5 m from the ship (Voss et al., 1986). In addition, the ship-induced light field perturbation and the influence of the ship shadowing and instrument self-shading on ocean irradiance profiles had been discussed in aspects of simulation and observation (Helliwell et al., 1990; Waters et al., 1990; Weir et al., 1994; Zibordi and Ferrari, 1995; Gordon and Ding, 1992). In our fieldwork, however, the influence of the platform *Zodiac* boat on the optical profiles was eliminated by performing two intercomparable experiments.

The main objective of this paper is to theoretically and practically assess the impacts of the ice cover on the ocean optics observations in the MIZ. We first introduce the field sampling strategy and the postprocessing of data in Section 2. In Section 3, the impacts of the platform *Zodiac* boat on the ocean optics profiles are analyzed. This assessment is comprehensively addressed in Section 4. Finally, we conclude this paper and provide some recommendations concerning the ocean optics observations in the MIZ in Section 5.

Foundation item: The National Natural Science Foundation of China under contract No. 41206174; China Postdoctoral Science Foundation under contract No. 2012M511546; the Chinese Polar Scinece Strategy Fund under contract No. 20110204.
*Corresponding author, E-mail: jpzhao@ouc.edu.cn

2 Methods

2.1 *Study area and equipment*

In situ assessment experiments were conducted in the Beaufort Sea during two periods in the summer of 2009: the period from 17 to 30 July, focusing on the effect of the ice cover on the optics measurements when the average ice concentration was 50%, and the other period from 11 September to 8 October , focusing on the impacts of the *Zodiac* boat (Fig. 1). The measurement instrument was Profiler II with hyperspectral ocean color radiometers (HyperOCR), which is the first of Satlantic's new line of hyperspectral instruments, providing up to 136 channels of optical data with wavelengths ranging from 350 to 800 nm. The SL70C radar, which is equipped with temperature, conductivity, pressure and inclination sensors, was used to measure the horizontal distances between the ice edge and the sensors with a minimum distance of 23 m.

2.2 *Measurement strategy*

At each station, an ice floe with an approximate area of bigger than 10 m×10 m was selected as the target. Optical sensors were then deployed at sites of 0–5 m, 25 m, 50 m, 100 m and 150 m away from the ice edge. These distances were determined by the SL70C pathfinder radar. To make the distance between the sensors and the ice edge as accurate as possible, it was necessary to gain the optical profiles as quickly as possible. Therefore, the sensors were put into the water 1 m away from the *Zodiac* boat (which was 7.3 m long) and then followed a free-fall release with a velocity of 0.4 m/s. Each cast lasted for approximately 2 min, as the deployment depth was approximately 50 m. However, data within the upper surface were unavoidably contaminated by the *Zodiac* boat. This contamination then required a calibration experiment to rectify the data.

The calibration measurements were made in an open water in September 2009. At Sta. 0926, three casts were taken at a particular site under overcast sky conditions: the first two profiles were collected consecutively with the sensors 20 m away from the boat, and the third profile was sampled at the same position with the sensors 1 m away from the boat. At Sta. 0929, two casts were performed under cloudy sky conditions: the sensors were 20 m away from the *Zodiac* for one cast and 1 m away from the Zodiac for the other cast. When the optical profiles were sampled, ancillary data and information such as the date, location, solar position, wind field and sky conditions were also recorded (Table 1).

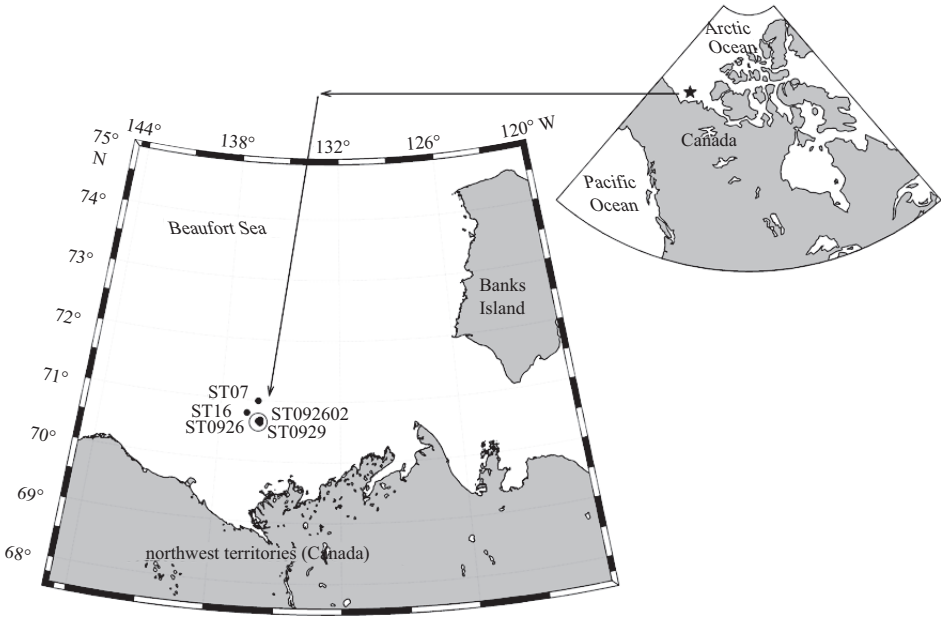

Fig.1. Study area in the southern Beaufort Sea in the Arctic Ocean. Three stations (ST0926, ST092602 and ST0929) are overlapped in this graph and marked by the black circle.

Table 1. Description of stations and instrumentation parameters in the field

Station ID	Date (locally)	Hours (locally)	Location		θ/(°)	φ/(°)	Wind		CS[1)]	Distances to ice edge/m[2)]
			North latitude	West longitude			Speed/m·s^{-1}	Dir./(°)		
ST16	Jul. 24	09:30–11:00	70°47.246'	136°40.564'	54.67	100–120	3.09	353	clear sky	2, 25, 50, 100
ST07	Jul. 25	10:00–11:15	70°59.270'	136°08.333'	53.56	–	4.63	85	overcast	5, 25, 50, 100, 150
ST0926	Sep. 26	14:00–15:00	70°39.500'	136°05.600'	76.55	–	1.03	320	overcast	no ice
ST092602	Sep. 26	15:00–16:00	70°40.503'	135°59.536'	78.30	–	1.03	320	overcast	no ice
ST0929	Sep. 29	14:30–16:00	70°37.606'	136°00.752'	79.45	–	3.60	20	cloudy sky	no ice

Notes: [1)] Abbreviation "CS" refers to "condition of sky". The θ and φ represent the solar zenith angle and relative azimuth angle, respectively. [2)] Distance to ice edge were estimated when the distance was less than or equal to 25 m.

2.3 *Postprocessing of data*

The dominant uncertainties in the spectral DAC profiles were primarily caused by changes in a cloud cover during the cast, resulting in strong variations in an incident surface irradiance $E_s[t(z),\lambda]$ measured at time $t(z)$. Furthermore, because of the spatial separation between the surface and underwater radiometers, cloud shadow variations were neither measured identically, nor in phase, by the two instruments. The $E_s[t(z),\lambda]$ profiles, therefore, needed to be smoothed to remove these high frequency fluctuations. In our case, a filtered period of 50 s was chosen according to the field environment.

Assuming that the transmission of $E_s[t(z),\lambda]$ through the surface does not vary with time, a simple and effective normalization of the profiles is obtained as

$$\hat{E}_d(z,\lambda)=\frac{E_d(z,\lambda)E_s[t(0^-),\lambda]}{E_s[t(z),\lambda]}, \tag{1}$$

where $E_s[t(z),\lambda]$ is the deck cell irradiance measured at time $t(z)$ when the underwater radiometer was at depth z; and $E_s[t(0^-),\lambda]$ is the irradiance measurement at time $t(0^-)$ when the radiometer was on the surface. To minimize the impact of waves at the surface, $E_s[t(5),\lambda]$ measured at time $t(5)$ was chosen instead of the $E_s[t(0^-),\lambda]$ measured at $t(0)$.

To compare the profiles taken from all the stations, the casts were normalized into a standard reference incident surface irradiance. In this study, these standard incident spectral irradiances were appointed to those during the first cast,

$$\tilde{E}_d(z,\lambda)=\frac{\hat{E}_d(z,\lambda)E_s[(t(5),\lambda)]}{E_{s_i}[(t(5),\lambda)]} \quad i=2,\ldots,5, \tag{2}$$

where subscript i represents the ith cast at each station.

Based on the Beer-Lambert law, the normalized $\tilde{E}_d(z,\lambda)$ should be fit to the equation

$$\tilde{E}_d(z,\lambda)=\tilde{E}_d(5,\lambda)e^{-\int_5^z K_d(z',\lambda)dz'}. \tag{3}$$

Taking the natural logarithm of Eq. (3) gives

$$-\int_5^z K_d(z')dz'=\ln\tilde{E}_d(z)-\ln\tilde{E}_d(5), \tag{4}$$

therefore,

$$K_d(z)=-\frac{d\ln[\tilde{E}_d(z)]}{dz}\Big|_z. \tag{5}$$

The traditional method of K-analysis, e.g., that of Smith and Baker (1984, 1986), is to estimate $K(z)$ as the local slope of ln $\tilde{E}_d(z,\lambda)$ measured within a depth interval spanning a few meters and'centered at depth z_m. It is assumed that $K(z)$ is constant over the depth interval centered at z_m, so that

$$\ln\tilde{E}(z)\approx\ln\tilde{E}(z_m)-(z-z_m)K(z_m), \tag{6}$$

The unknowns ln $\tilde{E}(z_m)$ and $K(z_m)$ are determined as the intercept and (negative) slope of a linear least-squares regression fit to the measured ln $\tilde{E}(z_m)$ data within the depth interval $(z_m-\Delta z)\leqslant z<(z_m+\Delta z)$.

$E_{PAR}(z)$, which is associated with a primary production, can be calculated from the spectral downwelling irradiance,

$$\begin{aligned}E_{PAR}(z)&=\frac{1}{Ahc}\int_{400}^{700}\lambda E_d(\lambda,z)d\lambda\\&\approx\frac{1}{Ahc}\left[\lambda_1E_d(\lambda_1,z)\frac{\lambda_2-\lambda_1}{2}+\lambda_nE_d(\lambda_n,z)\frac{\lambda_n-\lambda_{n-1}}{2}+\sum_{i=2}^{n-1}\lambda_iE_d(\lambda_i,z)\frac{\lambda_{i+1}-\lambda_{i-1}}{2}\right],\end{aligned} \tag{7}$$

where the units of the $E_{PAR}(z)$ and $E_d(z,\lambda)$ are μmol/(m^2·s) and W/(m^2·nm), respectively; A=6.02×10^{17} μmol^{-1}, h=6.62×10^{-34} W·s^2 (Planck's constant) and c=3.00 ×10^{17} nm/s (speed of light) (Mobley, 1994).

Analogously, $K_u(\lambda)$ and K_{PAR} were also calculated from the corrected $\tilde{L}_u(z,\lambda)$ and $E_{PAR}(z)$ following the method described above.

3 Impact assessment of the Zodiac boat on the cast

To minimize the displacement between the sensors and the ice edge caused by both surface currents and wind, the optical experiments were conducted in weak-wind conditions (Table 1), and the sensors were deployed against the boat to shorten the cast duration. Unfortunately, this deployment method led to the contamination of upper surface data by the boat.

In September 2009, two groups of experiments were carried out in the open water to examine the impact of the *Zodiac* boat on the optical measurements near the surface. In this study, we used the spectral DAC of the downwelling irradiance as a target quality to analyze the contamination of the *Zodiac* boat on the optical profiles. The spectral DAC, based on the ocean optics protocols developed by Mueller et al. (2002), is the negative local slope of the logarithmic downwelling irradiance, which is calculated following a linear least-square regression fit with the depth interval Δz=8 m.

At Sta. 0926, the first two profiles were expected to have the same trend because the casts were collected within 30 min of each other. However, a maximum difference in K_d of 0.005 m^{-1} was found between the two casts (Figs 2a and b). Here, we treated the difference of 0.005 m^{-1} as a systematic error to distinguish the impact of the *Zodiac* boat.

Under overcast sky conditions, the *Zodiac* boat affected the K_d profiles above the depth of 13 m when the sensors were put into the water 1 m away from the boat. If Profiler II was deployed on the side of the boat facing the Sun under a cloudy sky, the depth to which the *Zodiac* boat affected the K_d profiles was reduced to 10 m. It should also be noted that the optical profiles beneath the depth of $(h-\Delta z/2)$ are not influenced by an object on the surface if the spectral DACs are correct below the depth of h. In our case, the impact of the *Zodiac* boat on the ocean optical casts occurred only within the upper 9 m under overcast sky conditions and within the upper 6 m under cloudy sky conditions. Therefore, only data below the threshold (10 m or 6 m) were used for further analyses.

4 Impact assessment of ice cover on ocean optics observations

The ocean optics observations are commonly affected by the

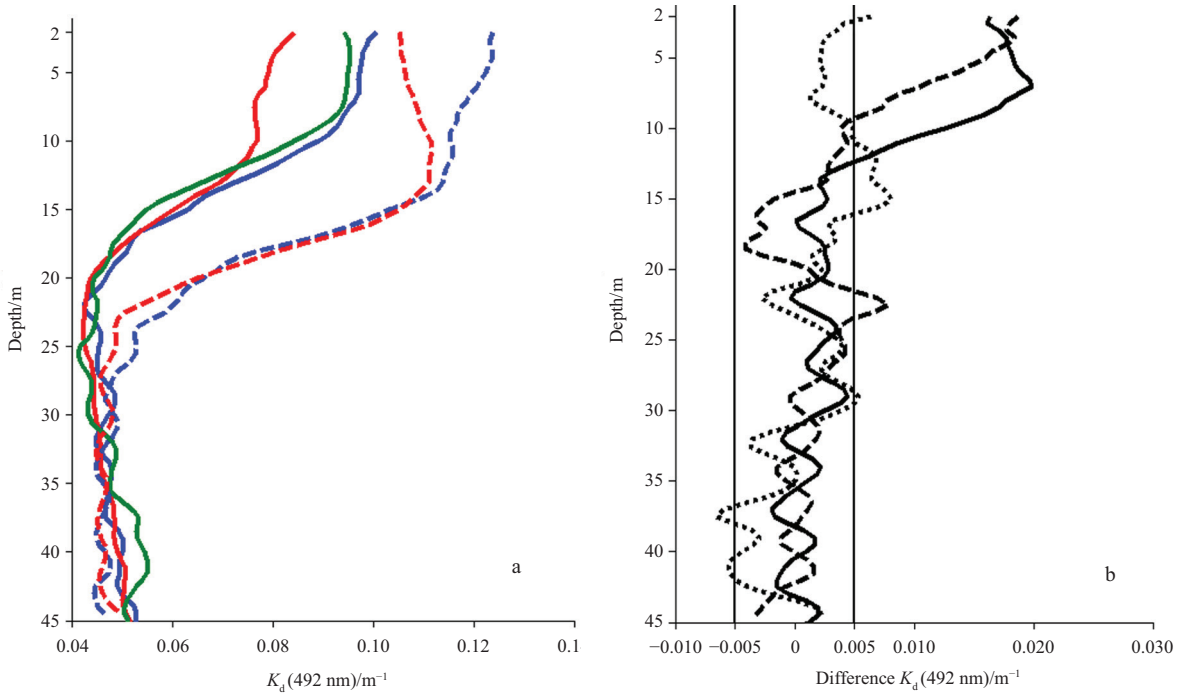

Fig.2. Investigation of the boat's impacts on the ocean optics observations. a. Profiles of DAC: blue solid line–far from the boat in overcast conditions (0926_far); blue dashed line–against the boat in overcast conditions (0926_near); red solid line–far from the boat in cloudy sky conditions (0929_far); red dashed line–against the boat in cloudy sky conditions (0929_near); and green solid line–far from the boat in overcast conditions (092602_far), and b. absolute error profiles of DAC: solid line–overcast conditions (0926_far–0926_near); dashed line–cloudy sky conditions (0929_far–0929_near); and doted line–profile of systematic error (difference between the 0926_far and 092602_far).

sea ice cover in polar regions, particularly in locations with a high ice concentration. These impacts are enlarged in the post-processing of data, resulting in some degree of error in calculating the optical properties of seawater, such as the spectral DACs. In this section, we first discuss the influence of the sea ice cover based on a geometric optics theory and compare the field measurements to the model. Then, the depth and extent of the impact of sea ice cover are investigated with *in situ* experiments in the southern Beaufort Sea.

4.1 *Theoretical model analysis*

Under clear sky conditions, we set up a local Descartes' coordinate system on sea ice with the solar zenith angle θ and the relative azimuth angle φ (Fig. 3, x axis not shown). According to geometric optics theory, if the horizontal distance between the sensors and the ice is L (in unit of m), then the upper boundary H of an ice shadow in water below which the sensors will be covered by sea ice is

$$H = -\frac{L/\cos\varphi + f\tan\theta}{\tan\theta'}, \tag{8}$$

where f is the freeboard of ice and θ' is the refraction angle in water obtained from Snell's law:

$$\frac{\sin\theta}{\sin\theta'} = \frac{n_w}{n_a}, \tag{9}$$

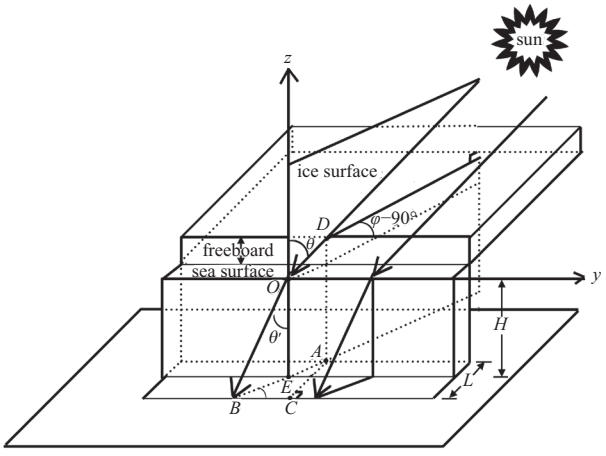

Fig.3. Schematic geometry defining the quantities used in the theoretical model. A collimating light with a zenith θ and a relative azimuth φ propagates into the water against to the ice edge, resulting in a shadow area ΔOBE. The initial shadow depth H is equal to the OE, whereas the distance of sensors to ice edge is AC.

in which n_w represents the refraction index of seawater, which is approximately equal to 1.34 for visible wavelengths; and n_a=1.0, the refraction index of air.

Assuming that f= 0.1 m in our case, H can be expressed by

$$H = -\frac{L/\cos\varphi + 0.1\tan\theta}{\tan\arcsin(\sin\theta/1.34)}. \quad (10)$$

In Eq. (10), the relative solar azimuth angle φ and the distance L can be measured *in situ*, meanwhile the zenith angle θ at a particular date and location can be calculated by

$$\cos\theta = \sin\phi\sin\delta + \cos\phi\cos\delta\cos H_a, \quad (11)$$

where ϕ is the local latitude; H_a is the hour angle; and δ is the solar declination. According to Liou's (2002) study, δ is given by

$$\sin\delta = \sin\left(\frac{23.5\pi}{180}\right)\sin\left(\frac{2\pi t_v}{365.24}\right), \quad (12)$$

where t_v are the days from the vernal equinox in a year. The hour angle H_a is defined as

$$H_a = \pi\frac{T_{solar} - 12}{12}, \quad (13)$$

where T_{solar} is the local solar hour, which is related to the coordinated universal time T_{UTC}, time equation E_t and local longitude β by

$$T_{solar} = T_{UTC} + E_t/60 + \beta/15, \quad (14)$$

where the E_t is given with Julian day n by the following equations:

$$E_t = \begin{cases} -14.2\sin\left(\pi\dfrac{n+7}{111}\right) & n = 1-106 \\ 4.0\sin\left(\pi\dfrac{n-106}{59}\right) & n = 107-166 \\ -6.5\sin\left(\pi\dfrac{n-166}{80}\right) & n = 167-246 \\ 16.4\sin\left(\pi\dfrac{n-247}{113}\right) & n = 247-365 \end{cases}. \quad (15)$$

To summarize the above equations, the initial shadow depth H can be estimated by Eq. (10) if the sampling date, time, location (longitude and latitude), relative solar azimuth angle and horizontal distance between the sensors and the ice edge are well known.

According to Eq. (10), depth H decreases as the solar zenith angle and the relative azimuth angle at a given horizontal distance L increase. In particular, there is a remarkable initial reduction in H when the relative azimuth angle is smaller than a certain φ_0 (Fig. 4a). Then, H experiences a stable shadowing at $\varphi>\varphi_0$. This conclusion is highly practicable in the field sampling. The depth H could be estimated accurately if an appropriate measuring geometry were set up to make the relative solar azimuth angle $\varphi>\varphi_0$. This set-up would improve the efficiency of the *in situ* measurements in polar ocean optics observations.

In the field, a relative solar azimuth angle φ of 135° is recommended as the standard value φ_0 because this angle is more convenient to set up and estimate than other relative solar azimuth angles. When the sensors are close to the ice edge, e.g., L=2 m (Fig. 4a), the depth H ranges from 4.8 to 6.9 m for θ=30° and from 0.8 to 1.5 m for θ=85° as 135°⩽φ⩽180°. Therefore, the smaller the distance L and the larger the zenith angle θ, the more accurate the estimation of depth H. In contrast, a small change in φ of 90°⩽φ⩽135° leads to a huge error in the estimated depth H (Figs 4a to d).

To test the theoretical model, an optical profile 2 m away from the ice edge under clear sky conditions with θ≈55° and 100°⩽φ⩽120° was chosen as an example. It was found that K_d reached a peak at a depth of 6.5 m (Fig. 5 red curves), indicating the strongest energy extinction in that layer and reflecting that the sensors were completely covered by sea ice beneath this depth. In fact, the initial depth H varied from 6 to 7 m as the profiles were processed into an intervals of 0.5 m. Using Eq. (10) with a depth range of 6–7 m, the calculated φ varied between 110° and 115°, which was within the range of the *in situ* values, 100°–120° (see Table 1). This result suggests that the geometric optics model is a practical method to estimate the initial shadow depth H.

Alternatively, the depth H is a linear function of distance L with a slope of $-[\cos\varphi\tan\arcsin(\sin\theta/1.34)]^{-1}$. With a particular solar position, the depth H increases as L extends away from the ice edge (Figs 4e to h). Additionally, the smaller the relative solar azimuth angle φ, the faster the increase in depth H. An analogous relationship between the depth H and the solar zenith angle θ is observed as well (Figs 4f to h).

4.2 *Impact assessments in the field experiments*

Although the theoretical model discussed above could provide a reference for the *in situ* sampling and data postprocessing, further efforts are still needed to consider the impacts of other factors on optics data, such as the solar azimuth angle and the transmitted radiative energy through ice. Furthermore, the geometric optics model works well with collimated illumination, but not with diffuse light fields, e.g., the overcast sky is common in the Arctic. Therefore, it is necessary to assess the effects of the ice cover on the *in situ* optical observations under both clear and overcast sky conditions.

Under clear sky conditions, radiative quantities such as spectral downwelling irradiance, upwelling radiance and $E_{PAR}(z)$ at a distance of 25 m from the ice edge were not affected by the ice cover with θ≈55° and 110°⩽φ⩽115° (dashed, dotted and dot-dashed curves in Figs 6a to c). These results led to unaffected derived quantities of spectral DACs (dashed, dotted and dot-dashed curves of the Figs 6d to f). Compared with the theoretical initial depth of 71–94 m from Eq. (10), in this case, the optical profiles in the upper 50 m should not be affected by the ice cover. If the theoretical initial shadow depth is set up to 50 m with the same solar position, then by Eq. (10), the impacts of the ice cover on the optical profiles could also be neglected in the upper 50 m in cases where the sensors were deployed 15 m away from the ice edge.

In the case where the sensors were deployed 2 m away from the ice edge, the sensors were shadowed beneath a depth of 6.5 m, resulting in sharp decreases in radiative quantities E_d, L_u and E_{PAR} (thick solid curves of Figs 6a to c). In contrast, beneath a particular depth, the spectral DACs were almost identical to those measurements unaffected by the ice cover, suggesting the quasi-inherent optical properties of seawater. These particular depths were 15 m for E_d (492 nm), 10 m for L_u (492 nm) and 15 m for E_{PAR} (Table 2). These results will aid in the field observations of quasi-inherent optical properties of seawater, such as spectral DACs, in areas of the Arctic with high ice concentrations.

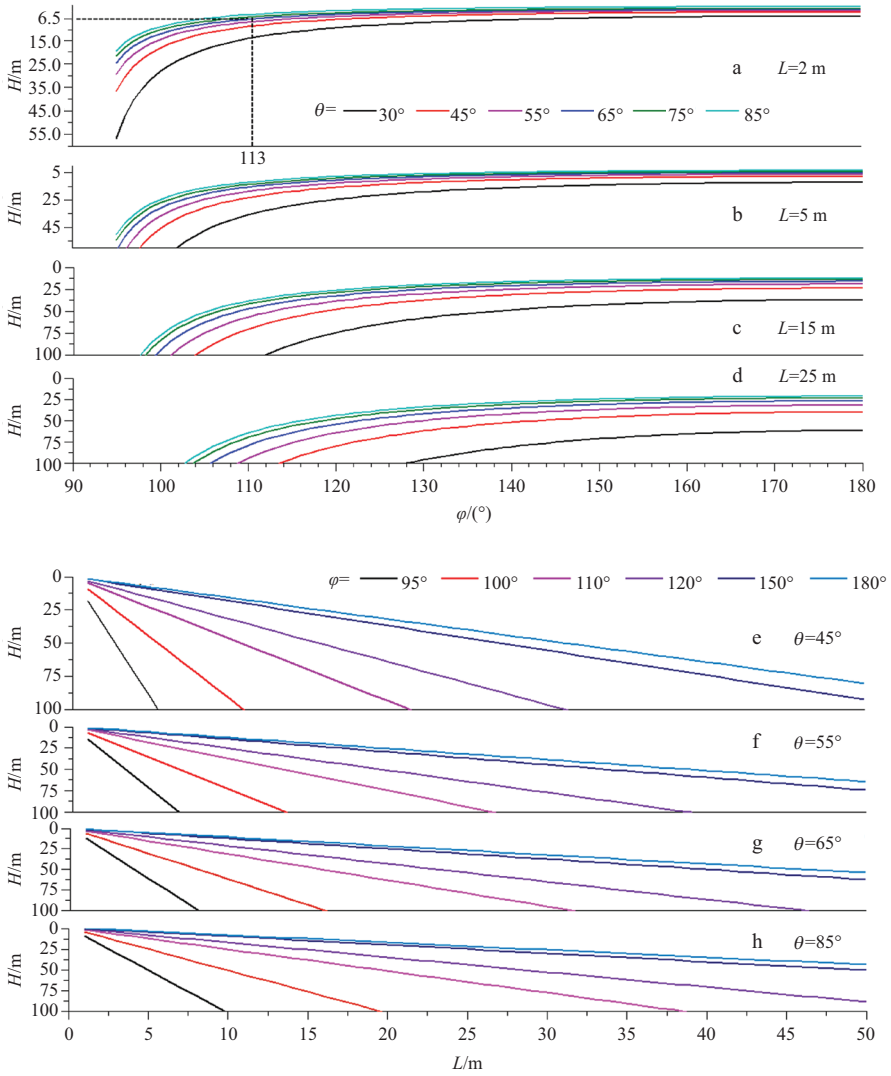

Fig.4. Initial depth affected by the ice cover varies with the solar zenith angle and the relative azimuth angle (a to d) and the horizontal distance of sensors to the ice edge (e to h). In Figs 4a to d, a remarkable initial reduction in H occurs, followed by a stable trend, with the solar azimuth angle of the sun at L=2 m (a), L=5 m (b), L=15 m (c) and L=25 m (d). In Figs 4e to h, H linearly increases as L increases at θ=45°(e), θ=55° (f), θ=65° (g) and θ=85° (h).

Table 2. Depth below which the profiles of DACs are unaffected by sea ice

Condition of sky (position of the profiler)	Depth for E_d (492 nm)/m	Depth for L_u (492 nm)/m	Depth for E_{PAR}/m
Clear sky (2 m to ice)	15	10	15
Overcast (5 m to ice)	35	27	35

Because there is no way to completely eliminate sea ice at these stations, some of the optical properties discussed above can be obtained as accurately as possible if instruments are completely deployed beneath the ice cover.

As overcast sky conditions occur frequently during the Arctic summer, it is important to assess the effects of the ice cover on ocean optics observations under the diffuse incident light fields. The results of the *in situ* experiments revealed that the profiles of both measured radiative quantities and calculated spectral DACs within the upper 50 m had the same trends when the sensors were more than 25 m away from the ice edge (dashed, dotted and dot-dashed curves in Figs 7a to c). When the horizontal distance between the sensors and the ice was 5 m, the directly measured radiative quantities were considerably smaller than those at a minimum of 25 m from the ice, which suggests the impact of the ice cover on the measured radiative quantities. However, the profiles of spectral DACs at 5 m from the ice had similar features to those at a distance of 2 m from the ice under clear sky conditions. These profiles were not affected by the ice cover beneath certain depths (thick solid curves in Figs 7d to f). In our fieldwork, these depths were 35 m for E_d (492 nm), 27 m for L_u (492 nm) and 35 m for E_{PAR} (Table 2). These depths were much deeper than those found under clear sky conditions. Although the smallest distance between the sensors and the ice

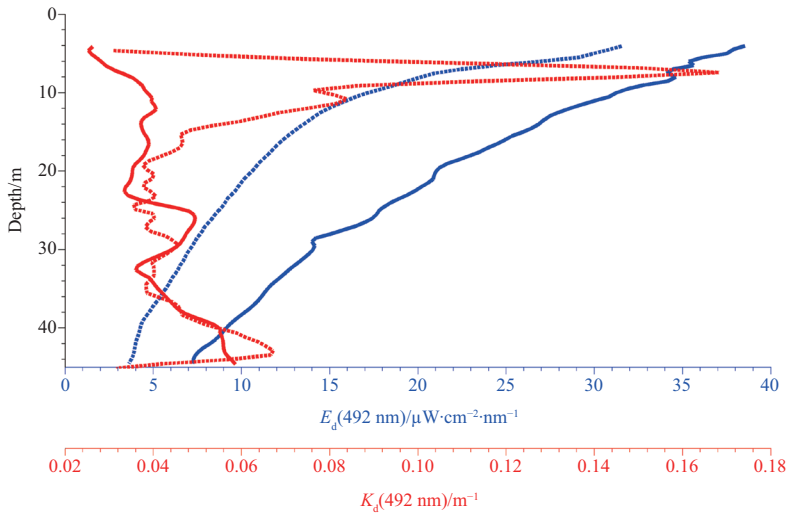

Fig.5. Profiles of downwelling irradiance and their DACs. The blue solid line represents E_d 100 m from the ice; the blue dashed line does E_d 2 m from the ice; the red solid line does K_d 100 m from the ice and the red dashed line does K_d 2 m from the ice.

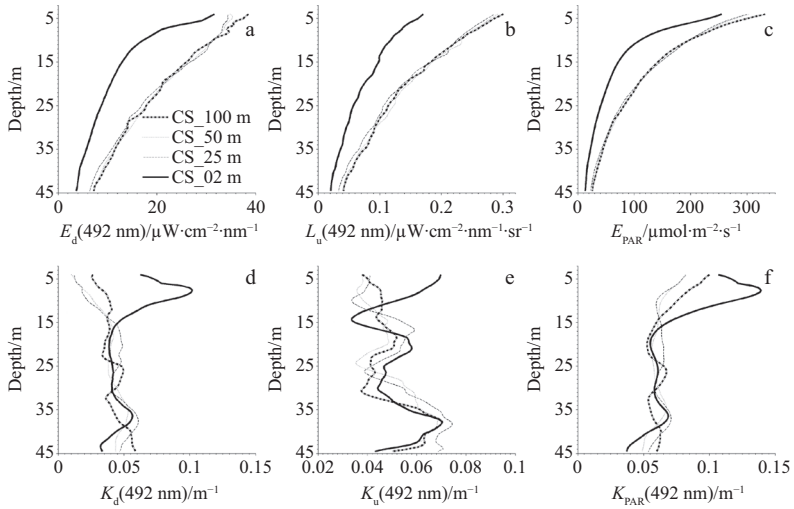

Fig.6. Profiles of E_d (a), L_u (b), E_{PAR} (c), K_d (d), K_u (e) and K_{PAR} (f) in collimated illumination conditions. CS_k in the legend means that the profile was taken at a site k away from the ice edge under clear sky conditions while the k=2, 25, 50 and 100 m.

at which the optical profiles within the upper 50 m would not be influenced by the ice cover remains unknown, we can confidently conclude that the profiles more than 25 m away from the ice edge reflect the practical light fields and optical properties of sea water under an overcast sky.

5 Conclusions

In the Arctic, the ocean optics observations to obtain the quasi-inherent optical properties of sea water, e.g., DAC, are often affected by the ice cover in regions with a high sea ice concentration. To avoid this contamination, optical instruments are typically deployed as far as possible from the ice edge. However, it is not practical to completely eliminate the impact of the ice cover at stations with an ice concentration of more than 90%. Therefore, it is necessary to quantitatively assess the role of the ice cover in the ocean optics experiments.

Based on the geometric optics theory, the upper boundary depth of the ice shadow in water under clear sky conditions can be calculated using the solar position according to the zenith and relative azimuth angles and the horizontal distance between the sensors and the ice edge. This depth could be obtained more accurately with a larger solar zenith angle and an empirical estimate of the relative azimuth angle ranging from 135° to 180°. Inversely, the relative solar azimuth angle could also be computed using the shadow boundary depth obtained from the observed profile data, the horizontal distance between the sensors and the ice and the station location.

In the field experiments with a solar position of $\theta \approx 55°$ and $110° \leqslant \varphi \leqslant 115°$, the spectral DACs of downwelling irradiance, upwelling radiance and $E_{PAR}(z)$ at a distance of 2 m from the ice

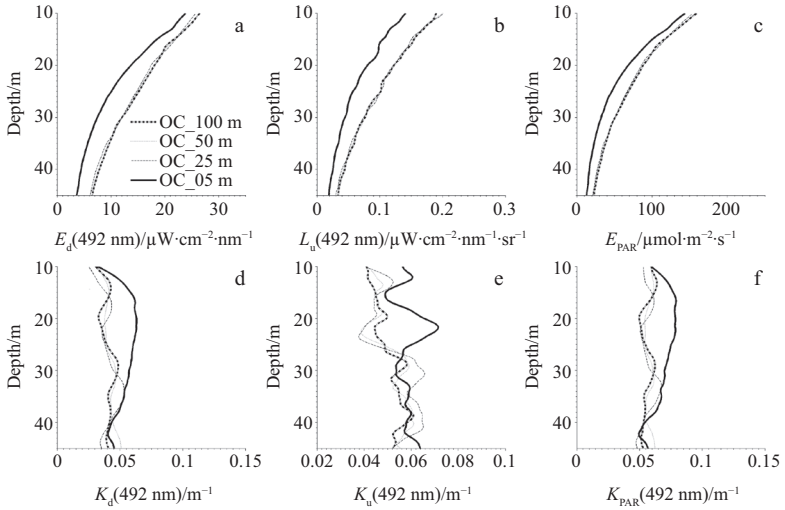

Fig.7. Profiles of E_d (a), L_u (b), E_{PAR} (c), K_d (d), K_u (e) and K_{PAR} (f) in diffuse illumination conditions. OC_*k* in the legend means that the profile was taken at a site *k* away from the ice edge under clear sky conditions while the *k*=5, 25, 50 and 100 m.

edge were not influenced by the ice cover beneath depth of 15 m, 10 m and 15 m, respectively. At sites more than 25 m away from the ice edge, the optical observations within the upper 50 m were not affected by the sea ice either, considering that the shortest theoretical horizontal distance was 15 m.

Under an overcast sky with a diffuse incident light field, neither the directly measured radiative quantities nor the calculated spectral DACs were contaminated by an ice shadow at sites more than 25 m away from the ice edge. At sites 5 m from the ice, the spectral DACs of downwelling irradiance, upwelling radiance and E_{PAR} were not affected by the ice cover beneath depths of 35 m, 27 m and 35 m, respectively.

An important conclusion drawn from these assessment experiments is that the spectral DACs of under-ice seawater can be calculated correctly with reasonable instrumentation. The total DACs, however, cannot be computed due to the impact of ice on the incident light field.

The findings in this study provide some useful information for the *in situ* ocean optics observations in the Arctic, particularly under overcast sky conditions. However, it should be noted that there have some cases of more than one piece of floe ice in the study area, which is not discussed in this paper. In those cases, we believe that the conclusions in this study could be most basic criteria to guide the ocean optics measurements in the polar area. The floe ice in this study should be one of the closest to the sensors while there have a few pieces of ice. Otherwise, making the instrument covered by sea ice completely also can obtain the accurate DACs of seawater. For clear sky conditions, the estimates of boundary depth and distance from the ice edge by which the accuracy of the observed spectral DACs are limited could be obtained from the theoretical geometric light model. However, these estimates still need be supported by further *in situ* data.

References

Deser C, Teng H Y. 2008. Evolution of Arctic sea ice concentration trends and the role of atmospheric circulation forcing, 1979–2007. Geophysical Research Letters, 35(2): L02504, doi: 10.1029/2007GL032023

Gordon H R. 1985. Ship perturbation of irradiance measurements at sea. 1: Monte Carlo simulations. Applied Optics, 24(23): 4172–4182

Gordon H R, Ding K Y. 1992. Self-shading of in-water optical instruments. Limnol Oceanogr, 118: 491–500

Haas C, Nicolaus M, Willmes S, et al. 2008. Sea ice and snow thickness and physical properties of an ice floe in the western Weddell Sea and their changes during spring warming. Deep Sea Research: Part II, 55(8–9): 963–974

Helliwell W S, Sullivan G N, Macdonald B, et al. 1990. Ship shadowing: model and data comparisons. In: Ocean Optics X Proceedings Orlando: SPIE, 55–71

Kwok R, Cunningham G F, Wensnahan M, et al. 2009. Thinning and volume loss of the Arctic Ocean sea ice cover: 2003–2008. Journal of Geophysical Research, 114(C7): C07005, doi: 10.1029/2009JC005312

Kwok R, Rothrock D A. 2009. Decline in Arctic sea ice thickness from submarine and ICESat records: 1958–2008. Geophys Res Lett, 36(15): L15501, doi: 10.1029/2009GL039035

Liou K N. 2002. An Introduction to Atmospheric Radiation. San Diego: Academic Press, 1210

Mobley C D. 1994. Light and Water: Radiative Transfer in Natural Waters. San Diego: Academic Press, 36–37

Mueller J L, Fargion G S, McClain C R, et al. 2002. Ocean Optics Protocols for Satellite Ocean Color Sensor Validation. Revision 4. Maryland: NASA, 13

Smith R C, Baker K S. 1984. The Analysis of Ocean Optical Data I, In: Ocean Optics VII Proceedings. Orlando: SPIE, 119–126

Smith R C, Baker K S. 1986. Analysis of Ocean Optical Data II. In: Ocean Optics VIII Proceedings. Orlando: SPIE, 95–107

Voss K J, Nolten J W, Edwards G D. 1986. Ship shadow effects on apparent optical properties. In: Ocean Optics VIII Proceedings. Orlando: SPIE, 186–190

Waters K J, Smith R C, Lewis M R. 1990. Avoiding ship-induced light-field perturbation in the determination of oceanic optical properties. Oceanography, 3(2): 18–21

Weir C T, Siegel D A, Michaels A F, et al. 1994. In situ evaluation of a ship's shadow. In: Ocean Optics XII Proceedings. Orlando: SPIE, 815–821

Zibordi G, Ferrari G M. 1995. Instrument self-shading in underwater optical measurements: experimental data. Applied Optics, 34(15): 2750–2754